

Learning Interactions Between Continuous Treatments and Covariates with a Semiparametric Model

Muyan Jiang

MUYAN_JIANG@BERKELEY.EDU

Computational Precision Health, University of California, Berkeley, USA

Department of Industrial Engineering and Operations Research, University of California, Berkeley, USA

Yunkai Zhang

YUNKAI_ZHANG@BERKELEY.EDU

Department of Industrial Engineering and Operations Research, University of California, Berkeley, USA

Anil Aswani

AASWANI@BERKELEY.EDU

Computational Precision Health, University of California, Berkeley, USA

Department of Industrial Engineering and Operations Research, University of California, Berkeley, USA

Abstract

Estimating the impact of continuous treatment variables (e.g., dosage amount) on binary outcomes presents significant challenges in modeling and estimation because many existing approaches make strong assumptions that do not hold for certain continuous treatment variables. For instance, traditional logistic regression makes strong linearity assumptions that do not hold for continuous treatment variables like time of initiation. In this work, we propose a semiparametric regression framework that decomposes effects into two interpretable components: a prognostic score that captures baseline outcome risk based on a combination of clinical, genetic, and sociodemographic features, and a treatment-interaction score that flexibly models the optimal treatment level via a nonparametric link function. By connecting these two parametric scores with Nadaraya-Watson regression, our approach is both interpretable and flexible. The potential of our approach is demonstrated through numerical simulations that show empirical estimation convergence. We conclude by applying our approach to a real-world case study using the International Warfarin Pharmacogenomics Consortium (IWPC) dataset to show our approach’s clinical utility by deriving personalized warfarin dosing recommendations that integrate both genetic and clinical data, providing insights towards enhancing patient safety and therapeutic efficacy in anticoagulation therapy.

Data and Code Availability This paper uses public data from the International Warfarin Pharmacogenomics Consortium (IWPC) on

the **Pharmacogenomics Knowledgebase (Whirl-Carrillo et al., 2021)**. Our code is available: <https://github.com/JimmyJiang666/Semiparametric-Regression-Treatment>.

Institutional Review Board (IRB) This research does not require IRB approval.

1. Introduction

In health-related decision-making, continuous treatments—such as dosing levels or intervention timing—play a critical role. However, estimating their impact on binary outcomes (e.g., treatment success or failure) remains a challenge. Traditional methods, such as logistic regression, impose rigid linearity assumptions that frequently fail to capture the complex, nonlinear interactions between treatment and patient-specific covariates (Thomas et al., 2014). In contrast, while flexible machine learning models like neural networks can capture these intricate relationships, their inherent lack of interpretability renders them less suitable for clinical settings where transparency is essential for trust and actionable decision-making.

In the context of continuous treatments and binary outcomes, regression models incorporating continuous treatment variables provide valuable insights into treatment-response dynamics, which are essential for optimizing interventions. Traditional approaches, such as logistic regression (Hosmer Jr et al., 2013), treat continuous treatments as linear covariates, imposing strong linearity assumptions that may fail to capture complex, nonlinear interactions between treat-

ments and patient-specific covariates. More advanced techniques, such as outcome-weighted learning, have been developed to refine personalized dosing strategies (Chen et al., 2016). Similarly, Kallus and Zhou (2018) introduced a framework for evaluating continuous treatment policies using kernel-enhanced inverse probability weighting and doubly robust methods, while Jin et al. (2023) proposed a change-plane model to identify and analyze subgroups with heterogeneous treatment effects. However, these methods often favor predictive accuracy over interpretability or trade transparency for flexibility, leading to complex models that hinder practical use in clinical settings.

Another related approach is the Generalized Propensity Score (GPS) method, which is useful for estimating causal effects of continuous treatments (Hirano and Imbens, 2004). GPS methods rely on correctly specifying a parametric model for the treatment assignment given the covariates, and any misspecification can lead to biased estimates of the dose-response function. Although nonparametric or machine learning techniques can be employed to mitigate this issue, they add further complexity to the analysis.

Semiparametric regression models offer a promising alternative by integrating the strengths of both parametric and nonparametric approaches. A classical example is the single index model, given by

$$\mathbb{E}(Y | X) = g(\xi^T X) + \epsilon,$$

which has been successfully applied in fields ranging from economics to healthcare, providing a compact and interpretable summary of complex relationships (Hristache et al., 2001; d’Haultfoeuille et al., 2022; Wang et al., 2020). The term “single index” refers to capturing covariate effects via the univariate projection $\xi^T X$, reducing dimensionality while maintaining flexibility through the nonparametric link function g . Unlike GLMs where g is predefined (e.g., logit or identity), here it is estimated nonparametrically, often with smoothness constraints like monotonicity or differentiability. A spline-based g , for instance, accommodates nonlinear relationships beyond the linear case $g(u) = u$. Though traditionally applied to continuous Y , extensions for binary outcomes make it a natural fit for our approach. Recent work has further extended these ideas to optimize treatment rules in clinical trials (Park et al., 2021, 2022b).

Building on these insights, our work proposes a semiparametric regression framework specifically tailored for settings with binary outcomes and continuous treatments. In our approach, the treatment

effect is decomposed into two interpretable components: a *prognostic score* that quantifies baseline risk and a *treatment-interaction score* that captures how patient covariates modulate the treatment effect. The unknown treatment-interaction function is modeled nonparametrically via a flexible function, estimated using Nadaraya–Watson regression with regularization to ensure both robustness and interpretability. Figure 1 provides an overview of our pipeline.

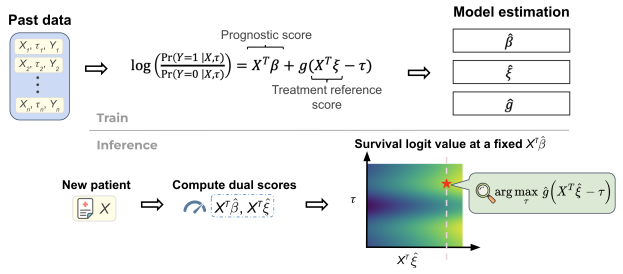


Figure 1: Overview of our proposed pipeline. During training, the model learns $\hat{\beta}$ and $\hat{\xi}$ associated prognosis and treatment effectiveness, respectively. During inference, as the prognostic score $X^T \hat{\beta}$ is fixed conditioning on the patient’s attributes, we can directly visualize outcome density using a heatmap with estimated \hat{g} . The optimal treatment value is then extrapolated at the maximum point along the y-axis corresponding to a fixed $X^T \hat{\xi}$.

The main contributions of this paper are as follows:

1. A partially linear model for estimating individualized treatment strategies that maintain interpretability through quantifying effects.
2. A dual-score framework comprising (i) a prognostic score capturing baseline outcome risk and (ii) a treatment-interaction score, providing actionable guidance for treatment assignment.
3. Numerical simulations under diverse scenarios demonstrating empirical convergence and robustness of the estimation method.
4. A real-world application to anticoagulation therapy data, showcasing the model’s utility in deriving personalized warfarin dosing recommendations.

2. Model Setup and Estimation

In clinical and observational studies, binary outcomes $Y \in \{0, 1\}$ (e.g., treatment success/failure) are often

analyzed alongside covariates $X \in \mathbb{R}^p$ and a continuous treatment variable $\tau \in \mathbb{R}$. While standard logistic regression treats τ as an additive covariate¹, this approach fails to address confounding—treatment assignment is often correlated with covariates, complicating effect estimation. To address this, we propose a model that explicitly incorporates treatment-covariate interactions while preserving interpretability through two clinically meaningful scores: a *prognostic score* capturing baseline risk using covariates (analogous to the linear predictor in logistic regression) and a *treatment-interaction score* guiding optimal τ assignment based on covariate-driven interactions.

2.1. Model Formulation

Given binary response $Y \in \{0, 1\}$, patient traits $X \in \mathbb{R}^p$, and treatment variable $\tau \in \mathbb{R}$, we consider the following logistic regression model:

$$\Pr(Y = 1|X, \tau) = \sigma(X^T \beta + g(X^T \xi - \tau)) \quad (1)$$

where $\sigma(\cdot) = \frac{1}{1+\exp(-\cdot)}$ is the logistic function, $g(\cdot) : \mathbb{R} \rightarrow \mathbb{R}$ is an unspecified function that models the effect of the treatment, and $\beta, \xi \in \mathbb{R}^p$ are learnable parameters. The first prognostic score $X^T \beta$ models the main linear effect based on the baseline traits of a patient. The second treatment-interaction score $X^T \xi$ is related to the treatment effect, where the difference term $X^T \xi - \tau$ is the argument of an unknown function g that encapsulates the covariates-treatment interaction. For instance, if $g(u) = u^2$, then $g(X^T \xi - \tau) = (X^T \xi - \tau)^2$, which introduces a multiplicative interaction between τ and $X^T \xi$, allowing the treatment effect to vary nonlinearly with patient covariates. Intuitively, $X^T \xi$ represents a patient-specific optimal treatment level derived from their covariates, and subtracting the actual treatment τ quantifies the deviation from this optimal level, which can be flexibly modeled by g . Furthermore, as we will discuss later, we normalize via $\xi \in \{\xi \in \mathbb{R}^p : \|\xi\|_2 = 1, \xi_1 \geq 0\}$ for identifiability because the function g is unknown and can absorb the scale and sign of ξ . Function g also needs to be learned alongside β and ξ .²

1. Note that our model is general and allows both positive and negative treatment values, although medical treatments are typically positive (e.g., drug dosage, radiation intensity). However, some cases, such as temperature modulation or ventilator pressure adjustments, may involve both signs.
2. Specifically, since g is estimated nonparametrically, any rescaling or sign reversal of ξ can be offset by a corresponding transformation of g , making ξ identifiable only up to scale and sign.

We consider the “odds ratio” (OR), a measure of association between a treatment and an outcome, and obtain the following:

$$\log \frac{\Pr(Y = 1|X, \tau)}{\Pr(Y = 0|X, \tau)} = X^T \beta + g(X^T \xi - \tau), \quad (2)$$

which reduces to a partially linear model with an unknown nonlinear part.

In a practical application, the prognostic score $X^T \beta$ highlights the pre-treatment condition, and the subsequent treatment-interaction score $X^T \xi$ is analyzed in conjunction with the function g , which elucidates the additive impact of the proposed treatment. Given data $\{X_i, Y_i, \tau_i\}_{i=1,\dots,n}$, denote $\bar{Y}_i = \log \frac{\Pr(Y_i=1|X_i, \tau_i)}{\Pr(Y_i=0|X_i, \tau_i)}$, $Z_i(\xi) = X_i^T \xi - \tau_i$ for a fixed ξ . Our partially linear model becomes

$$\bar{Y}_i = X_i^T \beta + g(Z_i(\xi)) + e_i, \quad (3)$$

where e_i is the error term with $\mathbb{E}(e_i|Z_i(\xi)) = 0$.

2.2. Proposed Estimation

In the above formulation, it remains to estimate parameters β, ξ and the unknown function g , which we denote as $\hat{\beta}, \hat{\xi}$, and \hat{g} respectively.

Condition Equation (3) on $Z_i(\xi)$, we obtain

$$\mathbb{E}(\bar{Y}_i|Z_i(\xi)) = \mathbb{E}(X_i^T \beta|Z_i(\xi)) + g(Z_i(\xi)). \quad (4)$$

Taking the difference of Equation (3) and Equation (4), we obtain the following least-squares (LS) regression:

$$e_{yi} = e_{xi}^T \beta + e_i \quad (5)$$

where $e_{yi} = \bar{Y}_i - \mathbb{E}(\bar{Y}_i|Z_i(\xi))$ and $e_{xi} = X_i - \mathbb{E}(X_i|Z_i(\xi))$.

Based on Equation (5), we can immediately compute an (infeasible) estimate of β for LS regression

$$\tilde{\beta}(\xi) = \left(\sum_i^n e_{xi} e_{xi}^T \right)^{-1} \sum_i^n e_{xi} e_{yi}^T.$$

Note that this estimate depends on a realized value of ξ so we denote $\tilde{\beta}(\xi)$ to make the dependency clear. However, this estimate is infeasible because the unknown conditional means must be estimated. We can estimate e_{xi}, e_{yi} using nonparametric kernel regression such as the Nadaraya-Watson (NW) estimator (Nadaraya, 1964; Watson, 1964) and obtain:

$$\bar{\beta}(\xi) = \left(\sum_i^n \hat{e}_{xi} \hat{e}_{xi}^T \right)^{-1} \sum_i^n \hat{e}_{xi} \hat{e}_{yi}^T, \quad (6)$$

213 where

$$\hat{e}_{xi} = X_i - \frac{\sum_{j \neq i}^n K_{h_i}(Z_j(\xi) - Z_i(\xi)) \cdot X_j}{\sum_{j \neq i}^n K_{h_i}(Z_j(\xi) - Z_i(\xi))}, \quad (7)$$

$$\hat{e}_{yi} = \bar{Y}_i - \frac{\sum_{j \neq i}^n K_{h_i}(Z_j(\xi) - Z_i(\xi)) \cdot \bar{Y}_j}{\sum_{j \neq i}^n K_{h_i}(Z_j(\xi) - Z_i(\xi))}. \quad (8)$$

215 Here, $K(\cdot) : \mathbb{R} \rightarrow \mathbb{R}^+$ is any kernel function
216 that satisfies $\int K(t)dt = 1$, $\int tK(t)dt = 0$, and
217 $0 < \int t^2 K(t)dt < \infty$. Typical choices include the
218 Epanechnikov kernel, $K(t) = \frac{3}{4}(1-t^2)\mathbb{1}_{\{|t| \leq 1\}}$, the
219 Gaussian kernel, $K(t) = \frac{1}{\sqrt{2\pi}}e^{-t^2/2}$, and other com-
220 monly used smoothing functions. The latter terms in
221 both Equation (7) and Equation (8) correspond to the
222 Nadaraya–Watson (NW) estimators, where h_i is the
223 selected bandwidth, which serves as a hyperparameter
224 that controls the degree of smoothing.

225 Note that an estimate of $\hat{\beta}$ depends on a given ξ , so
226 we first estimate $\hat{\xi}$ by minimizing estimated residuals
227 as follows:

$$\hat{\xi} = \operatorname{argmin}_{\xi} \sum_i^n (r_i(\xi))^2, \quad (9)$$

228 where $r_i(\xi) = \hat{e}_{yi} - \hat{e}_{xi}^T \bar{\beta}(\xi)$.

229 We then use the obtained $\hat{\xi}$ to compute the corre-
230 sponding $\hat{\beta} = \bar{\beta}(\hat{\xi})$ from Equation (6). Finally, we can
231 estimate \hat{g} in the following nonparametric way using
232 NW regression again:

$$\hat{g}(Z) = \frac{\sum_i^n K_{h_i}(Z_i(\hat{\xi}) - Z) \cdot (\bar{Y}_i - X_i^T \hat{\beta})}{\sum_i^n K_{h_i}(Z_i(\hat{\xi}) - Z)}. \quad (10)$$

233 This approach is implicitly an iterative procedure
234 for the parameter estimation. However, because of
235 the closed-form OLS solution for $\bar{\beta}(\xi)$ within the op-
236 timization process for ξ , we can effectively perform a
237 one-run optimization on ξ first, rather than alternat-
238 ing between the two parameter estimates. We show
239 its pseudocode in Algorithm 1 in the Appendix.

240 In this model, the coefficient ξ is identifiable only up
241 to scale and sign because the nonparametric function
242 g can absorb rescalings and sign changes of ξ , making
243 ξ unique only up to these transformations. To ensure
244 identifiability, we impose the constraint

$$\Theta = \{\xi = (\xi_1, \dots, \xi_p)^T \in \mathbb{R}^p \mid \|\xi\|_2 = 1, \xi_1 \geq 0\}.$$

245 In addition, LASSO regularization is incorporated to
246 promote sparsity in the estimation of ξ (Tibshirani,
247 1996; Hoerl and Kennard, 1970). This regularization
248 is particularly important in healthcare applications

where high-dimensional data are common. Sparsity
249 not only helps mitigate issues of multicollinearity but
250 also simplifies the model, allowing clinicians to easily
251 identify the most influential patient characteristics.
252 Therefore, on top of the constrained version of Equa-
253 tion (9), we add a lasso penalty to ξ and estimate the
254 model by optimizing the following:

$$\begin{aligned} \hat{\xi} = \operatorname{argmin}_{\xi} & \sum_i^n (r_i(\xi))^2 + \lambda \|\xi\|_1 \\ \text{s.t. } & \|\xi\|_2 = 1, \xi_1 \geq 0. \end{aligned} \quad (11)$$

Notably, we regularize ξ but not β because ξ captures
256 treatment-covariate interactions, which are often high-
257 dimensional and complex. In contrast, β models base-
258 line prognosis and is left unregularized to provide an
259 unbiased estimate, consistent with traditional logistic
260 regression. The bandwidth and lasso penalty λ are
261 hyperparameters tunable via cross-validation.

3. Numerical Simulations for Empirical Convergence Analysis

In our simulation study, we designed four scenarios
265 (summarized in Table 1) intended to systematically
266 evaluate the convergence of the proposed estimation
267 framework in different settings commonly encountered
268 in clinical studies. Scenarios 1 and 2 represent ran-
269 domized control trial (RCT)-like settings with simple
270 interaction patterns (constant and linear, respectively)
271 serving as baseline performance benchmarks. Scenario
272 3 simulates observational data to evaluate robustness
273 against confounding, with a more complex unimodal
274 interaction. Scenario 4 assesses the method’s ability to
275 handle high-dimensional mixed data (categorical and
276 continuous) and complex multimodal interactions.

3.1. Experimental Setup

For scenario 1 and 2, X are generated as a multi-
279 variate Gaussian distribution with random mean μ
280 and covariance matrix Σ where $\mu \sim \text{Unif}(-1, 1)^p$ and
281 $\Sigma = AA^T$ with $A \sim \text{Unif}(0, 1)^{p \times p}$. The treatment
282 variable is generated using a standard Gaussian dis-
283 tribution $\tau \sim \mathcal{N}(0, 1)$. For the parameters, we simulate
284 $\beta \sim \text{Unif}(-1, 1)^4$ and $\xi \sim \text{Unif}(\mathbb{Q}_1)$ where \mathbb{Q}_1 denotes
285 the first quadrant on the unit sphere due to the iden-
286 tifiability constraint. The treatment-covariate term
287 is constant in scenario 1 and linear in scenario 2. For
288 the constant term in scenario 1, it means treatment
289 assignment does not affect the outcome. The linear

Table 1: Setup of simulated scenarios.

| | Covariates Type | Partially Linear Interaction | Interaction Type | Intervention Setting |
|------------|--------------------------|--|------------------|----------------------|
| Scenario 1 | Continuous | $\bar{Y} = X^T \beta + 3$ | Constant | RCTs |
| Scenario 2 | Continuous | $\bar{Y} = X^T \beta + (X^T \xi - \tau)$ | Linear | RCTs |
| Scenario 3 | Continuous | $\bar{Y} = X^T \beta - 0.5 \log(X^T \xi - \tau)$ | Unimodal | Observational |
| Scenario 4 | Categorical & Continuous | $\bar{Y} = X^T \beta - 1.2 \cos(\pi \cdot (X^T \xi - \tau)) \cdot e^{-(X^T \xi - \tau)^2}$ | Multimodal | RCTs |

term in scenario 2 implies that the treatment acts linearly on the outcome, and the optimal treatment decision is always the extreme point within the feasible range of the treatment, depending on the coefficient sign of the variable. In both scenarios, we let $p = 8$.

For scenario 3, we mimic an observational setting in which the treatment variable is intrinsically influenced by the covariates, as illustrated in Figure 2. We simulate X_4 as an independent uniform random variable from -1 to 1: $X_4 \sim \text{Unif}(-1, 1)$. Then we simulate $X_1 = \sqrt{|X_4|} + \text{Unif}(-1, 1)$, $X_2 = 0.5 \times X_1 + \text{Unif}(-0.5, 0.5)$, $X_3 = 0.3 \times X_1 + 0.3 \times X_2 + \text{Unif}(-0.4, 0.4)$ which are correlated. For the treatment, we have $\tau = \sin(X_2 X_3) + \text{Unif}(-0.6, 0.6)$, which are influenced by covariates X_2 and X_3 . Similarly, we simulate $\beta \sim \text{Unif}(-1, 1)^4$ and $\xi \sim \text{Unif}(Q_1)$. Lastly, for the interaction term, we have $\bar{Y} = X^T \beta - 0.5 \log(|X^T \xi - \tau|)$, where the optimal treatment is an unimodal function in the logarithmic term.

Notably, scenario 3 differs from the others in that τ explicitly depends on X_2 and X_3 , as illustrated in a causal Directed Acyclic Graph (DAG) Figure 2. This setup mirrors an observational study where treatment assignment is influenced by patient characteristics. In contrast, in all other scenarios, τ is independent of the covariates, resembling an RCT. Moreover, the treatment-covariates interaction function in scenario 3 assumes a unique optimal treatment captured by the log function with the argument in absolute value. The assumption is that for every patient, given the covariates, there exists a unique optimal treatment that maximizes the outcome variable.

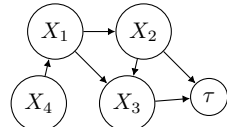


Figure 2: Directed Acyclic Graph in scenario 3.

For scenario 4, we want to simulate our covariates as a mixture of categorical and continuous variables in an RCT setting where the treatment variable is independent of the covariates. Let n_c, n_b denote the num-

ber of continuous and binary variables. We simulate $X_c \sim \mathcal{N}(\mu_c, \Sigma_c)$ with $\mu_c \in \mathbb{R}^{n_c}, \Sigma_c \in \mathbb{S}_{+}^{n_c}$, similarly as in scenario 1 and 2. For binary variables, we simulate $X_b[1] \sim \text{Bernoulli}(p_1)$ with $p_1 \sim \text{Unif}(0, 1)$. For $i = 2, \dots, n_b$, we simulate $X_b[i] = \text{Bernoulli}(p_i)$ with $p_i = \frac{1}{1 + \exp(-(a_i X_b[i-1] + b_i))}$. For each subsequent binary variable $X_b[i]$, its Bernoulli probability p_i is determined using a logistic function applied to a linear combination of the previous binary variable $X_b[i-1]$. The coefficients a_i and b_i in the logistic function can be adjusted to control the strength of the dependency. Notice that the treatment is generated independent of the covariates to resemble an RCT scenario. In our generation, we set $n_c = 12, n_b = 8, a_i = 0.5, b_i = -0.25$, to imitate realistic clinical datasets where continuous covariates typically outnumber categorical ones, reflecting more extensive clinical measurements compared to binary indicators (e.g., conditions or genotypes). The parameters a_i and b_i were chosen to induce moderate dependencies among categorical variables, realistically representing clinically plausible correlation structures without creating overly strong collinearity. We generate $\tau \sim \text{Unif}(-1, 1)$ independent of the covariates for the treatment. The treatment-covariates interaction term in scenario 4 involves some trigonometric and exponential functions. This creates some multimodal locally optimal treatment decisions, which can be seen in the heatmap of scenario 4 in Figure 3.

Table 1 summarizes the design for all scenarios. We estimated the model for each scenario using the constrained optimization framework as delineated in Equation (11). We investigated and implemented a range of optimization strategies, including classical methods such as Differential Evolution (Storn and Price, 1997) and CMA-ES (Hansen and Ostermeier, 2001). After assessing their performance in terms of computational efficiency, convergence behavior, and the ability to explore constrained search spaces, we ultimately implemented the Tree-based Parzen Estimators (TPE) algorithm via the *hyperopt* library (James Bergstra et al., 2013). This probabilistic optimization framework, as described in (Watanabe, 2023), is well-suited for this problem as it adaptively models the

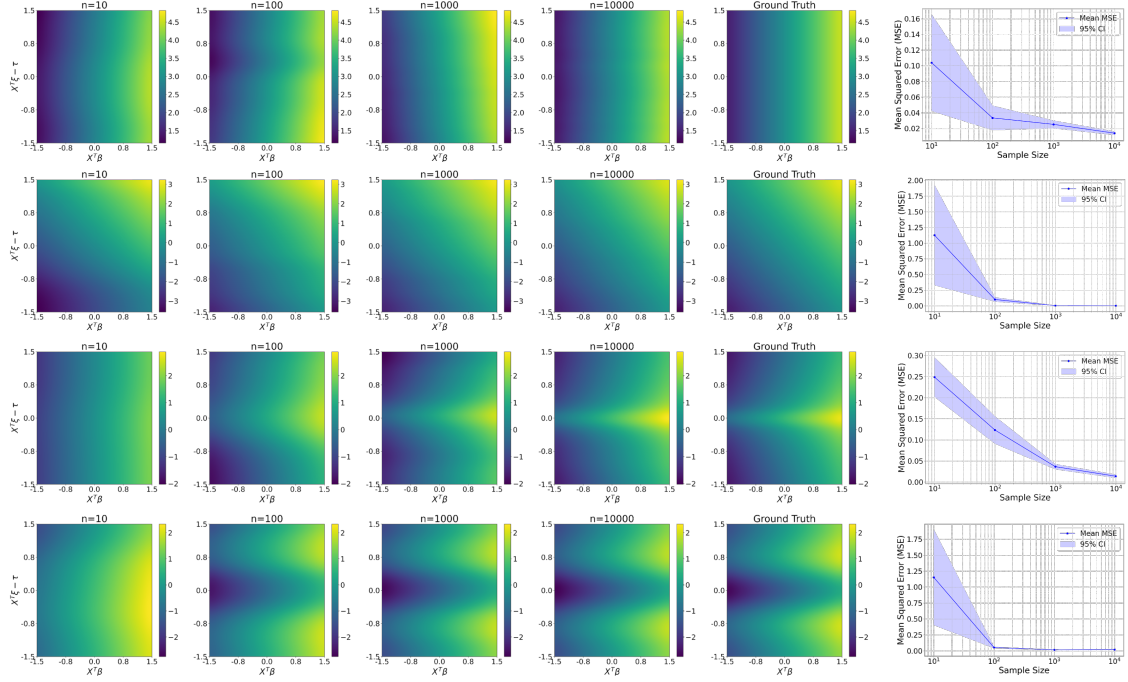


Figure 3: Empirical Convergence of Estimations. The four rows represent scenario 1-4, respectively. The heatmaps show estimated values of the modeled function across two dimensions: the prognostic score ($X^T \beta$, x-axis) and the covariate-treatment term ($X^T \xi - \tau$, y-axis). The colored density of the heatmap represents $\bar{Y} = \log \frac{Pr(Y=1|X,\tau)}{Pr(Y=0|X,\tau)}$, the log-odds ratio, where higher values indicate a greater likelihood of the positive outcome. Columns in the heatmap panel represent increasing sample sizes ($n = 10$ to 10^4), illustrating progressive convergence towards the true underlying function, shown in the rightmost (Ground Truth) column. The far-right plots quantify convergence through Mean Squared Error (MSE), bootstrapped ten times for confidence intervals. Note that the scale of the MSE y-axis differs between scenarios for visual clarity.

370 objective function's landscape using a probabilistic
371 approach, efficiently focusing on high-promise regions
372 while respecting the defined constraints on $\xi \in \Theta$.
373 Unlike unconstrained algorithms that may propose
374 solutions outside the feasible space or inefficiently ex-
375 plore irrelevant regions, TPE ensures that estimates
376 remain within the valid domain.

377 For clarity, the simulations assess empirical con-
378 vergence to the ground-truth function rather than
379 predictive accuracy via train-test splits. Each sce-
380 nario generates independent samples ($n = 10$ to 10^4)
381 to evaluate estimation consistency. Hyperparameters
382 (λ, h) are selected via cross-validation at each sample
383 size. Since the focus is on convergence, all generated
384 samples are used for estimation, and accuracy is mea-
385 sured using the mean squared error (MSE), defined as
386 $\int (\hat{g}(Z) - g(Z))^2 dZ$. This integral quantifies the devia-
387 tion between the estimated and true function over the

388 entire domain, making it a natural metric for assessing
389 convergence. The far right column in Figure 3 reports
390 MSE trends with bootstrapped confidence intervals.

3.2. Results and Discussion

392 In scenario 1, characterized by a constant interac-
393 tion term, convergence towards the ground truth
394 is achieved swiftly, even with a limited number of
395 training samples. Notably, with $n = 10000$, the es-
396 timated heatmap accurately reflects the treatment's
397 non-influence, maintaining a consistent scale along
398 the y-axis. A similar result is observed in scenario 2,
399 where the interaction term follows a linear pattern.
400 This linear relationship manifests as a diagonal gra-
401 dient in the heatmap, where the effect of treatment
402 changes proportionally with the covariate-treatment
403 interaction score. Scenario 3, featuring an unimodal
404 interaction term, requires a larger sample size to align

with the ground truth. This unimodal effect is visible in the heatmap as a single yellow band, indicating the unique optimal treatment level for different patient covariates. Starting from $n = 1000$, the estimation progressively discerns the unique optimal treatment, as captured by the logarithmic function. Scenario 4 introduces increased dimensionality, more complex data types, and a multimodal interaction term. The presence of multiple optimal treatment levels is reflected in the heatmap by two distinct yellow bands, illustrating the multimodal nature of the treatment response. The estimation necessitates a larger number of samples to achieve empirical convergence and discern multimodality in optimal treatment decisions.

For all scenarios, MSE decreases consistently as the sample size increases. Scenarios 1–3 exhibit notably lower MSE compared to Scenario 4, reflecting their simpler interaction structures and lower dimensionality. Importantly, our estimation framework demonstrates empirical convergence across diverse data types (continuous and binary covariates) and settings (RCTs and observational). Although observational data typically pose challenges due to confounding, which can reduce accuracy, we observe successful convergence in our simulations. Note that our observational scenario employs a simplified confounding structure; thus, further study with more complex, realistic confounding is needed to fully assess the method’s robustness in practical settings.

4. Application to Personalized Warfarin Dosing

We evaluate our semiparametric regression framework on a real-world dataset from the International Warfarin Pharmacogenomics Consortium (IWPC) (Whirl-Carrillo et al., 2021) to provide insights on individualized warfarin dosing strategies that enhance therapeutic efficacy, by integrating diverse clinical and genetic data. This dataset consists of 6000 patients. Warfarin is a critical anticoagulant with a narrow therapeutic range, where personalized dosing is essential due to marked inter-individual variability in drug response (Kim et al., 2015). The challenge of optimal dosing is particularly critical in intensive care and other high-risk settings, where rapid and precise dose adjustments are essential for patient safety.

The cohort selection process is shown in Figure 4. The selected cohort is divided into train and test sets with a ratio of 9:1. We extracted 30 covariates with both clinical and pharmacogenetic variables, in-

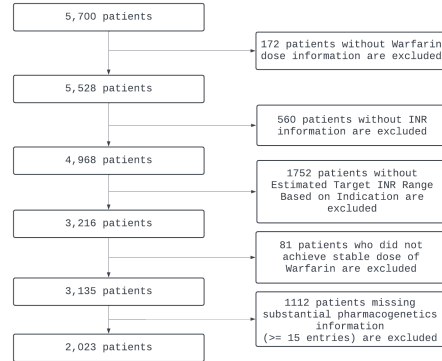


Figure 4: Cohort selection in the IPWC dataset.

cluding physical attributes, medical conditions, concomitant medications, genotype status of functional warfarin genetic polymorphisms, etc. Variables were selected based on their clinical relevance to warfarin metabolism, as informed by prior pharmacogenetic studies (Dietz et al., 2020; Wang et al., 2021; Kim et al., 2015), as well as non-missingness in the dataset. Additionally, feature importance analysis from the soft label distillation process (see Section 4.1) also guided the inclusion of predictive covariates. In particular, we included CYP2C9 and VKORC1 polymorphisms due to their well-documented roles in warfarin metabolism. CYP2C9 encodes a cytochrome P450 enzyme that metabolizes warfarin, with variants (*2, *3) reducing enzymatic activity, slowing clearance, and increasing bleeding risk. VKORC1 encodes warfarin’s target, vitamin K epoxide reductase, with variants (497, 1173, 1542, 1639, 3730) affecting enzyme expression and dose requirements. These markers were selected based on their established clinical relevance in pharmacogenetic studies. In practice, pharmacogenetic-guided dosing can improve dosing effectiveness in highly sensitive responders versus that of patients who received fixed-dose (Dietz et al., 2020). The International Normalized Ratio (INR) is a standardized measure of blood coagulation used to monitor the effectiveness of warfarin therapy. It represents the ratio of a patient’s prothrombin time to a control sample. Maintaining an INR within the appropriate target range is crucial to balancing the risk of clotting and bleeding. Different from studies that considered a fixed target INR (Park et al., 2022a), we constructed a binary outcome that indicates whether a patient’s INR falls within their personalized target range. This individualization is important since for deep vein thrombosis and atrial

fibrillation, the target is 2.0–3.0; for high-risk heart valve patients, it's above 3.0; a 1.5–2.0 range is recommended for some heart valve patients to reduce bleeding risks (Puskas et al., 2018).

In this study, our objective *diverges from* intensively refining the accuracy of warfarin dosage predictions, as explored in previous research (Chen et al., 2023; Wang et al., 2021; Lee et al., 2021). Instead, our model focuses on the ability to simultaneously quantify the patient's baseline risk via the prognostic score and delineate the optimal treatment level through the treatment-interaction score.

4.1. Distillation of Soft Labels

Because only binary labels are available for training, this causes the left-hand side of Equation (3), $\bar{Y}_i = \log \frac{Pr(Y_i=1|X_i, \tau_i)}{Pr(Y_i=0|X_i, \tau_i)}$, to be ill-defined. To address this issue, we train an intermediary model and then use the prediction of each sample (i.e., soft labels) in lieu of the binary ground truth to construct \bar{Y}_i . We refer to this intermediary model as the “expert model” and our model as the “student model” following Hinton et al. (2015). In our implementation, we used XGBoost (Chen and Guestrin, 2016) as the expert model.

For preprocessing, we normalized continuous variables and one-hot encoded categorical ones. Due to label imbalance (negative samples 12%), we applied SMOTE (Chawla et al., 2002) to achieve a 1:1 ratio. The expert model's performance is shown in the top-left panel of Figure 5. The expert model assigns soft labels used to train the student model.

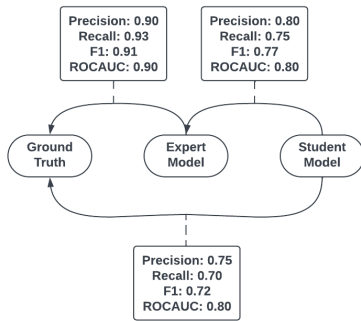


Figure 5: Predictive performance comparison. The arrow indicates the comparison's truth benchmark.

4.2. Student Model Training

We aligned the train, validation, and test split with the expert model and estimated the student model. To reduce computational load, we chose the Epanechnikov kernel $K(t) = \frac{3}{4}(1-t^2)\mathbb{1}_{\{|t|\leq 1\}}$ for its finite support, limiting computations to local neighborhoods. In practice, kernel choice had minimal impact on results, provided a reasonable bandwidth was used.

We tuned the two key hyperparameters in our model—the kernel bandwidth h and the LASSO penalty parameter λ —using 5-fold cross-validation, selecting values that minimized the average mean squared error (MSE). See Appendix B.4.1 for the sensitivity analysis on these two hyperparameters.

As a classification model, the student model's performance is constrained by the expert model because the student model does not have direct access to the ground truth and is only trained by the expert model, as shown in Figure 5. Using a more sophisticated and well-specified expert model may improve the accuracy.

4.3. Comparison on Other Prognostic Scores

In our model, $X^T\beta$ provides a prognostic score of the patient. This term can be analogized to the linear predictor in logistic regression. We compare the prognostic score estimation between our model and other linear models that offer similar insights, including Logistic Regression (LR) and Linear Discriminant Analysis (LDA), each with a variant in which the treatment variable is incorporated as a continuous covariate.

The comparison in Figure 6 demonstrates that, while there is general agreement in the direction of coefficients across models, our model exhibits notable differences in magnitude and confidence intervals for certain features. Specifically, our model moderates the influence of genetic polymorphisms, often shrinking their estimated effect toward zero, while assigning greater weight to clinical variables such as height, weight, and comorbidities (e.g., diabetes, use of statins). This suggests that our method prioritizes clinically relevant factors over genetic markers, which may have important implications for personalized treatment strategies.

Traditional models like LR and LDA assume a simple additive relationship between features and outcomes, while our approach explicitly incorporates non-linear treatment-covariate interactions. Consequently, these differences lead to variations in coefficient estimates and confidence intervals. This reflects different

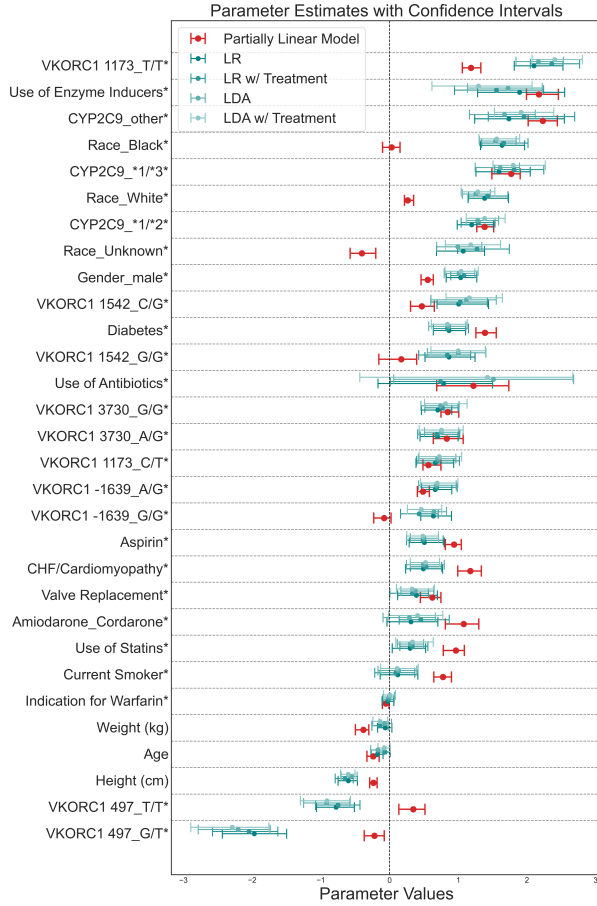


Figure 6: Linear prognostic score comparison. Attributes are ordered by the magnitude of the LR coefficient estimates. Categorical features are marked with an asterisk sign.

modeling choices rather than limitations of any single method.

While these models are fundamentally different in structure, we compare them not to establish correctness but to illustrate how different modeling choices influence prognostic scores derived from quantifiable coefficients. Since no single model serves as an absolute benchmark for correctness, our goal is to open up the discussion on how different modeling frameworks yield different prognostic estimates, each with its own interpretability and clinical implications. Future work will involve consulting with domain experts to assess the clinical plausibility of our findings and validate the model's utility in real-world treatment decisions.

4.4. Clinical Interpretations of Estimates

Figure 7 and 8 show the estimated coefficients with bootstrapped confidence intervals with $k = 30$ iterations.

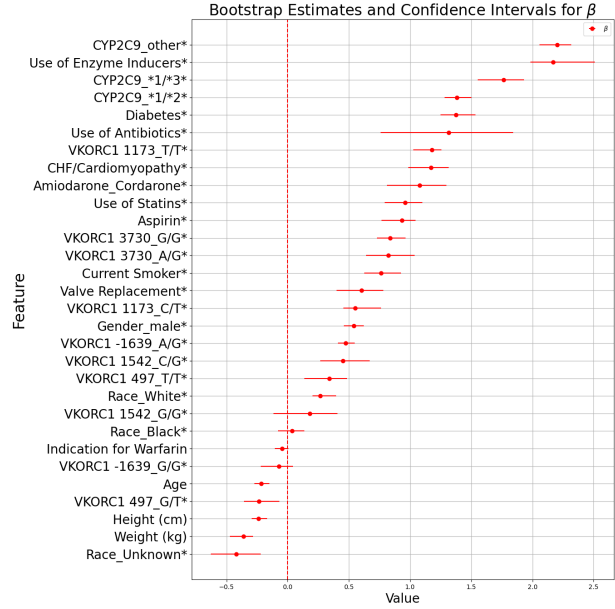


Figure 7: Values of β . Attributes are ordered by the magnitude of the corresponding coefficient estimates. Categorical features are marked with an asterisk sign.

For $X^T\beta$, Figure 7 indicates that larger values for “age”, “height”, and “weight” have a negative association with pre-treatment and may adversely affect the patient’s ability to achieve the target INR range. This effect may be attributed to higher values for these variables generally corresponding to larger body sizes. Additionally, specific genotypes, such as variants of CYP2C9, are linked to diminished enzyme activity. Individuals carrying these alleles typically metabolize warfarin more slowly, thereby facing a higher risk of bleeding at conventional doses. Consequently, they often necessitate a lower warfarin dose to attain the target range.

For the analysis of the treatment-interaction score $X^T\xi$ in relation to the treatment τ , we need to examine the function g at a fixed value of $X^T\beta$ to isolate its effect. As illustrated in Figure 9, a higher warfarin dose is beneficial for patients with scores from -1.0 to 0.5. Conversely, for those with scores above 1.0, a significantly lower dosage is recommended. Therefore, in Figure 8, the substantial negative coefficient associated with “age” suggests that older patients typically

require lower warfarin doses to achieve therapeutic INR levels. This observation aligns with existing literature that indicates that older patients are more sensitive to warfarin [Shendre et al. \(2018\)](#) and have an increased risk of bleeding complications ([Fihn et al., 1996](#)), necessitating lower doses for the same therapeutic effect. Likewise, the substantial negative coefficient associated with “weight” suggests that higher body weight typically requires higher warfarin doses to regulate their INR levels. Indeed, [Alshammari et al. \(2020\)](#) found that obese patients required approximately 20% higher weekly doses of warfarin compared to those with normal BMI and for each 1-point increase in BMI, the weekly warfarin dose increased by 0.69 mg ([Mueller et al., 2014](#)). Furthermore, the negative coefficient for “valve replacement” indicates that patients with typical valve replacements might require slightly higher warfarin doses, in accordance with current guidelines that recommend targeting INR of 2.5 to 3.5 for such patients ([Vahanian et al., 2022](#)), likely due to the increased risk of thromboembolic events associated with mechanical heart valves ([Carnicelli, 2015](#)).

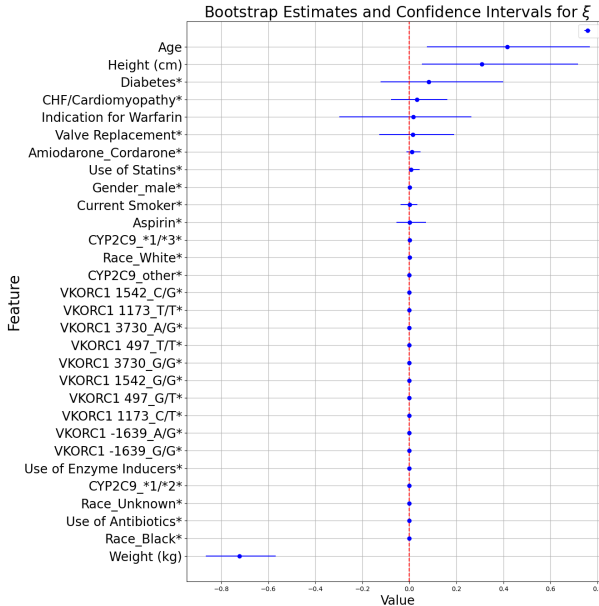


Figure 8: Estimated values of ξ . Attributes are ordered by the magnitude of their corresponding coefficient estimates. Categorical features are marked with an asterisk sign. A LASSO penalty is applied to ξ . Here, regularization eliminated over half the variables, highlighting the most relevant covariates for treatment effect modulation.

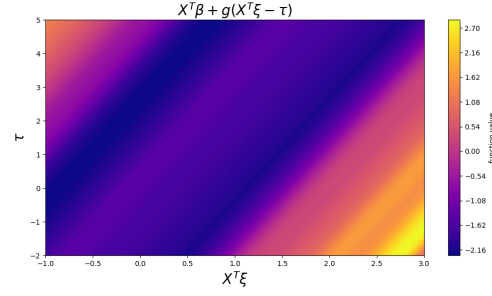


Figure 9: Estimated density function at $X^T \beta = 0.5$. The highlighted yellow region indicates improved outcomes with the corresponding treatment level τ .

5. Discussion and Conclusion

This study proposes a modified partially linear model to simultaneously estimate the direct linear effects of patient covariates and a nonlinear term capturing covariate-treatment interactions. The model employs NW regression for parameter estimation and to uncover the unknown link function. Numerical simulations demonstrate empirical convergence of the estimation procedure, and the model is applied to the International Pharmacogenetics Warfarin Consortium (IPWC) dataset, focusing on Warfarin dosing decisions and their impact on achieving the target International Normalized Ratio (INR) range.

The study has several limitations. First, the parameter estimation method is primarily empirical and lacks theoretical guarantees for consistency and reliability. Nonetheless, given our numerical experiments, we believe that the estimator is indeed statistically consistent, and our future work includes theoretically studying the statistical consistency properties of our proposed approach. Second, confounder selection and feature engineering could benefit from domain-specific expertise to improve robustness. The model’s clinical interpretability and practical values also require validation through prospective studies. Third, extending the framework to longitudinal data would better capture temporal dynamics in medical settings. Additionally, adapting the proposed framework to handle multi-class classification outcomes could be achieved by generalizing the logistic link function into multinomial logistic regression, thus enabling the modeling of multiple distinct clinical outcomes simultaneously. On top of that, generalizing the treatment variable to a multi-dimensional construct could enhance clinical utility in complex decision-making scenarios. Lastly,

666 while our approach balances interpretability and efficiency,
 667 a deeper comparison with more complicated methods like deep learning models and Bayesian optimization approaches is needed to assess scalability
 668 and computational trade-offs.

671 6. Acknowledgements

672 This material is based upon work supported by the National Science Foundation under Grant No. DGE-
 673 2125913 and Grant No. CMMI-1847666.

675 References

- 676 Abdullah Alshammari, Abdullah Altuwayjiri, Ziad Alshaharani, Rami Bustami, and Hind S Almodaimegh. Warfarin dosing requirement according to body mass index. *Cureus*, 12(10), 2020.
- 677 Anthony Carnicelli. Anticoagulation for valvular heart disease, 2015. URL <https://www.acc.org/latest-in-cardiology/articles/2015/05/18/09/58/anticoagulation-for-valvular-heart-disease>. Accessed: 2025-03-14.
- 678 Nitesh V Chawla, Kevin W Bowyer, Lawrence O Hall, and W Philip Kegelmeyer. Smote: synthetic minority over-sampling technique. *Journal of artificial intelligence research*, 16:321–357, 2002.
- 679 Guanhua Chen, Donglin Zeng, and Michael R Kosorok. Personalized dose finding using outcome weighted learning. *Journal of the American Statistical Association*, 111(516):1509–1521, 2016.
- 680 Richard J Chen, Judy J Wang, Drew FK Williamson, Tiffany Y Chen, Jana Lipkova, Ming Y Lu, Sharifa Sahai, and Faisal Mahmood. Algorithmic fairness in artificial intelligence for medicine and healthcare. *Nature biomedical engineering*, 7(6):719–742, 2023.
- 681 Tianqi Chen and Carlos Guestrin. Xgboost: A scalable tree boosting system. In *Proceedings of the 22nd ACM SIGKDD international conference on knowledge discovery and data mining*, pages 785–794, 2016.
- 682 Xavier d’Haultfoeuille, Christophe Gaillac, and Arnaud Maurel. Partially linear models under data combination. Technical report, National Bureau of Economic Research, 2022.
- 683 Nicholas Dietz, Christian Ruff, Robert P Giugliano, Michele F Mercuri, and Elliott M Antman. Pharmacogenetic-guided and clinical warfarin dosing algorithm assessments with bleeding outcomes risk-stratified by genetic and covariate subgroups. *International Journal of Cardiology*, 317:159–166, 2020.
- 684 Nick Erickson, Jonas Mueller, Alexander Shirkov, Hang Zhang, Pedro Larroy, Mu Li, and Alexander Smola. Autogluon-tabular: Robust and accurate automl for structured data. *arXiv preprint arXiv:2003.06505*, 2020.
- 685 Stephan D Fihn, Catherine M Callahan, Donald C Martin, Mary B McDonell, Jorja G Henikoff, Richard H White, and National Consortium of Anticoagulation Clinics*. The risk for and severity of bleeding complications in elderly patients treated with warfarin. *Annals of internal medicine*, 124(11):970–979, 1996.
- 686 Nikolaus Hansen and Andreas Ostermeier. Completely derandomized self-adaptation in evolution strategies. *Evolutionary computation*, 9(2):159–195, 2001.
- 687 Byeongho Heo, Minsik Lee, Sangdoo Yun, and Jin Young Choi. Knowledge distillation with adversarial samples supporting decision boundary. In *Proceedings of the AAAI conference on artificial intelligence*, volume 33, pages 3771–3778, 2019.
- 688 Geoffrey Hinton, Oriol Vinyals, and Jeff Dean. Distilling the knowledge in a neural network, 2015.
- 689 Keisuke Hirano and Guido W. Imbens. The propensity score with continuous treatments. *Applied Bayesian Modeling and Causal Inference from Incomplete-Data Perspectives*, pages 73–84, 2004.
- 690 Arthur E Hoerl and Robert W Kennard. Ridge regression: Biased estimation for nonorthogonal problems. *Technometrics*, 12(1):55–67, 1970.
- 691 David W Hosmer Jr, Stanley Lemeshow, and Rodney X Sturdivant. *Applied logistic regression*. John Wiley & Sons, 2013.
- 692 Marian Hristache, Anatoli Juditsky, and Vladimir Spokoiny. Direct estimation of the index coefficient in a single-index model. *Annals of Statistics*, pages 595–623, 2001.

- 751 James Bergstra, Dan Yamins, and David D. Cox.
 752 Hyperopt: A Python Library for Optimizing
 753 the Hyperparameters of Machine Learning Algo-
 754 rithms. In Stéfan van der Walt, Jarrod Millman,
 755 and Katy Huff, editors, *Proceedings of the 12th*
 756 *Python in Science Conference*, pages 13 – 19, 2013.
 757 doi:[10.25080/Majora-8b375195-003](https://doi.org/10.25080/Majora-8b375195-003).
- 758 Peng Jin, Wenbin Lu, Yu Chen, and Mengling Liu.
 759 Change-plane analysis for subgroup detection with a
 760 continuous treatment. *Biometrics*, 79(3):1920–1933,
 761 2023.
- 762 Nathan Kallus and Angela Zhou. Policy evaluation
 763 and optimization with continuous treatments. In
 764 *International conference on artificial intelligence*
 765 and statistics
- 766 Seongho Kim, Adam E Gaweda, Dongfeng Wu, Lang
 767 Li, Shesh N Rai, and Michael E Brier. Simplified
 768 warfarin dose-response pharmacodynamic models.
 769 *Biomedical Engineering: Applications, Basis and*
 770 *Communications*, 27(01):1550001, 2015.
- 771 Eric B Laber and Ying-Qi Zhao. Tree-based methods
 772 for individualized treatment regimes. *Biometrika*,
 773 102(3):501–514, 2015.
- 774 Heemoon Lee, Hyun Joo Kim, Hyoung Woo Chang,
 775 Dong Jung Kim, Jonghoon Mo, and Ji-Eon Kim.
 776 Development of a system to support warfarin dose
 777 decisions using deep neural networks. *Scientific*
 778 *Reports*, 11(1):14745, 2021.
- 779 Julia A Mueller, Tulsi Patel, Ahmad Halawa, Adrian
 780 Dumitrescu, and Nancy L Dawson. Warfarin dosing
 781 and body mass index. *Annals of Pharmacotherapy*,
 782 48(5):584–588, 2014.
- 783 Elizbar A Nadaraya. On estimating regression. *The-
 784 ory of Probability & Its Applications*, 9(1):141–142,
 785 1964.
- 786 Hyung Park, Eva Petkova, Thaddeus Tarpey, and
 787 R Todd Ogden. A constrained single-index regres-
 788 sion for estimating interactions between a treatment
 789 and covariates. *Biometrics*, 77(2):506–518, 2021.
- 790 Hyung Park, Eva Petkova, Thaddeus Tarpey, and
 791 R Todd Ogden. A single-index model with a surface-
 792 link for optimizing individualized dose rules. *Jour-
 793 nal of Computational and Graphical Statistics*, 31
 794 (2):553–562, 2022a.
- 795 Hyung Park, Thaddeus Tarpey, Mengling Liu, Keith
 796 Goldfeld, Yinxian Wu, Danni Wu, Yi Li, Jinchun
 797 Zhang, Dipayan Ganguly, Yogiraj Ray, et al. De-
 798 velopment and validation of a treatment benefit
 799 index to identify hospitalized patients with covid-19
 800 who may benefit from convalescent plasma. *JAMA*
 801 *network open*, 5(1):e2147375–e2147375, 2022b.
- 802 John D Puskas, Marc Gerdisch, Dennis Nichols, Lili-
 803 beth Fermin, Birger Rhenman, Divya Kapoor, Jack
 804 Copeland, Reed Quinn, G Chad Hughes, Hormoz
 805 Azar, et al. Anticoagulation and antiplatelet strate-
 806 gies after on-x mechanical aortic valve replacement.
 807 *Journal of the American College of Cardiology*, 71
 808 (24):2717–2726, 2018.
- 809 Aditi Shendre, Gaurav M Parmar, Chrisly Dillon,
 810 Timothy Mark Beasley, and Nita A Limdi. Influence
 811 of age on warfarin dose, anticoagulation control, and
 812 risk of hemorrhage. *Pharmacotherapy: The Journal*
 813 *of Human Pharmacology and Drug Therapy*, 38(6):
 814 588–596, 2018.
- 815 Rainer Storn and Kenneth Price. Differential
 816 evolution—a simple and efficient heuristic for global
 817 optimization over continuous spaces. *Journal of*
 818 *global optimization*, 11:341–359, 1997.
- 819 Doneal Thomas, Sanyath Radji, and A. Benedetti.
 820 Systematic review of methods for individual pa-
 821 tient data meta-analysis with binary outcomes.
 822 *BMC Medical Research Methodology*, 14:79–79, 2014.
 823 doi:[10.1186/1471-2288-14-79](https://doi.org/10.1186/1471-2288-14-79).
- 824 Robert Tibshirani. Regression shrinkage and selec-
 825 tion via the lasso. *Journal of the Royal Statistical*
 826 *Society: Series B (Methodological)*, 58(1):267–288,
 827 1996.
- 828 Alec Vahanian, Friedhelm Beyersdorf, Fabien Praz,
 829 Milan Milojevic, Stephan Baldus, Johann Bauer-
 830 sach, Davide Capodanno, et al. 2021 esc/eacts
 831 guidelines for the management of valvular heart
 832 disease. *European Heart Journal*, 43(7):561–632,
 833 2022.
- 834 Yuyan Wang, Yinxian Wu, Melanie H Jacobson,
 835 Myeonggyun Lee, Peng Jin, Leonardo Trasande,
 836 and Mengling Liu. A family of partial-linear single-
 837 index models for analyzing complex environmen-
 838 tal exposures with continuous, categorical, time-to-
 839 event, and longitudinal health outcomes. *Environ-
 840 mental Health*, 19:1–16, 2020.

| | | | |
|-----|--|---|---------------|
| 841 | Zeyuan Wang, Josiah Poon, Jie Yang, and Simon Poon. Warfarin dose estimation on high-dimensional and incomplete data. 2021. | Appendix Contents | 861 |
| 844 | Shuhei Watanabe. Tree-structured parzen estimator: Understanding its algorithm components and their roles for better empirical performance. <i>arXiv preprint arXiv:2304.11127</i> , 2023. | A Algorithm Overview | 14 862 |
| 848 | Geoffrey S Watson. Smooth regression analysis. <i>Sankhyā: The Indian Journal of Statistics, Series A</i> , pages 359–372, 1964. | B Further Discussion on Experiments | 14 863 |
| 851 | Michelle Whirl-Carrillo, Rachel Huddart, Li Gong, Katrin Sangkuhl, Caroline F Thorn, Ryan Whaley, and Teri E Klein. An evidence-based framework for evaluating pharmacogenomics knowledge for personalized medicine. <i>Clinical Pharmacology & Therapeutics</i> , 110(3):563–572, 2021. | B.1 Experiment Settings | 14 864 |
| 854 | | B.2 Simulation | 15 865 |
| 857 | | B.3 Warfarin Dosing Study | 15 866 |
| 859 | | B.4 Sensitivity Analysis | 15 867 |
| 860 | | B.4.1 Different Hyperparameters . . | 15 868 |
| | | B.4.2 Different Optimization Algorithms | 869 |
| | | | 16 870 |
| | | C Comparison with Existing Methods | 16 871 |

872 **Appendix A. Algorithm Overview**

873 We provide Algorithm 1 as an outline of the estimation
874 method used for our semiparametric regression
875 framework. The algorithm estimates the model pa-
876 rameters β , ξ and the nonparametric function g from
877 the data $\{(X_i, Y_i, \tau_i)\}_{i=1}^n$ using kernel regression and
878 constrained optimization with LASSO regularization.

879 **Appendix B. Further Discussion on
880 Experiments**

881 **B.1. Experiment Settings**

882 In the four simulation scenarios, the number of fea-
883 tures are 8, 8, 4, and 20, respectively. Among them,
884 scenario 4 has 8 categorical features, while the first
885 three scenarios only have numerical features. For each
886 scenario, $n = \{10, 10^2, 10^3, 10^4\}$ samples are gener-
887 ated from the distribution specified in Table 1 as the
888 train set. Instead of using a conventional test set, we
889 compute the mean squared error (MSE) directly with
890 the true function over the entire domain, defined as
891 $\int (\hat{g}(Z) - g(Z))^2 dZ$.

892 In our Warfarin dosing study, the dataset origi-
893 nally comprised 21 features before one-hot encoding.
894 Among these, 4 features are continuous numerical
895 variables: Age, Height (cm), Weight (kg), and Indi-
896 cation for Warfarin. There are 9 binary categorical
897 features that serve as direct yes/no indicators: Di-
898 abetes, CHF/Cardiomyopathy, Valve Replacement,
899 Aspirin, Amiodarone_Cordarone, Current Smoker,
900 Use of Statins, Use of Enzyme Inducers, and Use of
901 Antibiotics. Finally, 8 features were originally multi-
902 category variables that were one-hot encoded. These
903 include Gender (e.g., male/female), Race (with cate-
904 gories such as Black, Unknown, and White), CYP2C9
905 (with its multiple allelic variants), and five separate
906 VKORC1 genetic markers (namely -1639, 497, 1173,
907 1542, and 3730). The feature space comprises 30
908 dimensions (after one-hot encoding of categorical vari-
909 ables). The train set has 3177 samples, which are
910 obtained after applying augmentation via SMOTE,
911 and the test set has 353 samples.

912 There are two main hyperparameters in the pro-
913 posed algorithm, a bandwidth parameter h as well
914 as a regularization parameter λ . h is selected from
915 $\{0.15, 0.2, 0.25, 0.3, 0.35, 0.4\}$ and λ is selected from
916 $\{1 \times 10^{-5}, 1 \times 10^{-4}, 1 \times 10^{-3}, 1 \times 10^{-2}, 1 \times 10^{-1}\}$. We
917 used 5-fold cross-validation for hyperparameter tuning.
918 More details on the sensitivity to these hyperparame-

Algorithm 1 Semiparametric Estimation via Con-
strained Optimization

Require: Data $\{(X_i, Y_i, \tau_i)\}_{i=1}^n$; kernel $K(\cdot)$; band-
width h ; regularization parameter λ .

Ensure: Estimates $\hat{\beta}$, $\hat{\xi}$, and $\hat{g}(\cdot)$.

- 1:
- Compute Log-Odds:**
- $\bar{Y}_i \leftarrow \log \left(\frac{Pr(Y_i=1|X_i, \tau_i)}{Pr(Y_i=0|X_i, \tau_i)} \right)$
-
- 2: Define the search space:

$$\Theta = \left\{ \xi \in \mathbb{R}^p : \|\xi\|_2 = 1, \xi_1 \geq 0 \right\}.$$

- 3:
- Optimize ξ :**
- Find

$$\hat{\xi} \leftarrow \arg \min_{\xi \in \Theta} L(\xi),$$

where the objective function is defined as

$$L(\xi) = \sum_{i=1}^n [r_i(\xi)]^2 + \lambda \|\xi\|_1,$$

with

$$r_i(\xi) = \hat{e}_{yi}(\xi) - \hat{e}_{xi}(\xi)^T \bar{\beta}(\xi).$$

For each candidate ξ , compute:

$$\begin{aligned} Z_i(\xi) &= X_i^T \xi - \tau_i, \\ \hat{e}_{xi}(\xi) &= X_i - \hat{E}[X_i | Z_i(\xi)], \\ \hat{e}_{yi}(\xi) &= \bar{Y}_i - \hat{E}[\bar{Y}_i | Z_i(\xi)], \end{aligned}$$

where $\hat{E}[\cdot | Z]$ is estimated via Nadaraya–Watson
regression, and the least-squares estimate:

$$\bar{\beta}(\xi) = \left(\sum_{i=1}^n \hat{e}_{xi}(\xi) \hat{e}_{xi}(\xi)^T \right)^{-1} \sum_{i=1}^n \hat{e}_{xi}(\xi) \hat{e}_{yi}(\xi).$$

- 4:
- Finalize β :**
- Set
- $\hat{\beta} \leftarrow \bar{\beta}(\hat{\xi})$
- .
-
- 5:
- Estimate $g(\cdot)$:**
- For any
- Z
- , compute

$$\hat{g}(Z) = \frac{\sum_{i=1}^n K\left(\frac{Z_i(\hat{\xi}) - Z}{h_i}\right) (\bar{Y}_i - X_i^T \hat{\beta})}{\sum_{i=1}^n K\left(\frac{Z_i(\hat{\xi}) - Z}{h_i}\right)},$$

with $Z_i(\hat{\xi}) = X_i^T \hat{\xi} - \tau_i$.

- 6:
- return**
- $\hat{\beta}$
- ,
- $\hat{\xi}$
- , and
- $\hat{g}(\cdot)$
- .
-
- 7:
- Inference:**
- Return dual score
- $\{X_k^T \hat{\beta}, X_k^T \hat{\xi}\}$
- , pre-
-
- diction
- $\text{sign}(X_k^T \hat{\beta} + \hat{g}(X_k^T \hat{\xi} - \tau_k))$
- , and counterfac-
-
- tual optimal treatment
- $\tilde{\tau} = \arg \max_{\tau} \hat{g}(X_k^T \hat{\xi} - \tau)$
- .

919 ter choices are shown in Appendix B.4.1. In particular,
 920 for the TPE algorithm implemented via Hyperopt, we
 921 set `max_evals` = 200 to ensure thorough exploration
 922 of the parameter space.

923 All experiments were conducted locally on a Mac-
 924 Book Pro equipped with an Apple M3 chip with an
 925 8-core CPU (4 high-performance cores and 4 energy-
 926 efficient cores) and 16GB of unified memory, using
 927 Python 3.9 and PyTorch.

928 B.2. Simulation

929 For illustration purposes, we also include a plot for
 930 scenario 3 and 4 with the learned classification decision
 931 boundary from the training data and the distribution
 932 of the test samples in Figure 10. We observe that
 933 all the misclassified samples are located along the
 934 decision boundary, where the samples overlap.

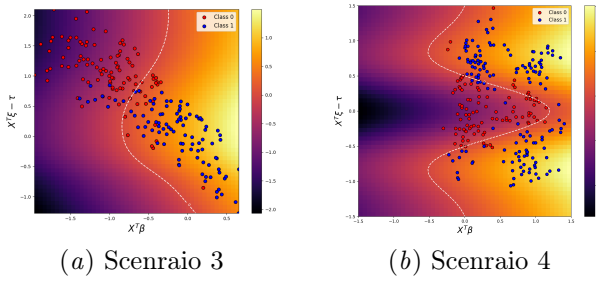


Figure 10: Learned classification decision boundaries for scenario 3 and scenario 4. The dashed white line indicates the decision boundary where the function value is zero, and the heatmap density represents the log-odds (higher values indicate a greater likelihood of a positive outcome).

935 Granted, the model’s classification performance is
 936 limited by its suboptimal decision boundary. For
 937 improved distillation, knowledge transfer strategies
 938 targeting decision boundaries—such as adversarial
 939 attacks to refine boundary-critical samples—may war-
 940 rant exploration (Heo et al., 2019).

941 B.3. Warfarin Dosing Study

942 We first compare standard linear models—Logistic
 943 Regression (LR) and Linear Discriminant Analysis
 944 (LDA)—along with their variants that incorporate
 945 the treatment variable as a continuous covariate (de-
 946 noted as “LR/LDA with τ ”). In Section 4.3, we assess
 947 the clinical interpretability of their prognostic scores,

Table 2: Performance comparison of linear models offering prognostic scores. Recall that our model is distilled from the non-interpretable expert model XG-Boost, so we also include its scores here as a reference. Our model will likely improve further with a stronger expert model.

| Model | Precision | Recall | F1 | AUC |
|------------------------|--------------|--------------|--------------|--------------|
| LR | 0.646 | 0.697 | 0.671 | 0.775 |
| LR with τ | 0.651 | 0.705 | 0.677 | 0.788 |
| LDA | 0.671 | 0.697 | 0.684 | 0.779 |
| LDA with τ | 0.650 | 0.684 | 0.667 | 0.789 |
| Our Model | 0.747 | 0.704 | 0.725 | 0.784 |
| XGBoost (Reference) | 0.902 | 0.925 | 0.913 | 0.904 |

where $X^T \beta$ serves as an analog to the linear predictor in logistic regression. To provide a more comprehensive evaluation, we also examine their predictive performance on classification tasks. Table 2 summarizes key metrics (precision, recall, F1, and ROC AUC), highlighting the effectiveness of our proposed model relative to these standard approaches.

945 B.4. Sensitivity Analysis

946 B.4.1. DIFFERENT HYPERPARAMETERS

947 Our proposed algorithm has two hyperparameters, a
 948 bandwidth parameter h as well as a regularization
 949 parameter λ . We performed a sensitivity analysis
 950 on these two hyperparameters using the Warfarin
 951 (IWPC) dataset. The results are shown in Figure 11.
 952 The top subfigure shows the average MSE over five
 953 runs, while the bottom subfigure shows the average
 954 training time. In the plots, green circles indicate
 955 lower MSE or faster training times, while red circles
 956 indicate higher MSE or longer training times. An “X”
 957 marks any hyperparameter combination for which the
 958 algorithm failed to converge.

959 Our analysis shows that our algorithm can achieve
 960 competitive MSE levels under a wide range of hy-
 961 perparameters ($h \in [0.2, 0.4]$ and $\lambda \in [10^{-5}, 10^{-2}]$),
 962 demonstrating its robustness to different hyperpar-
 963 ameter settings. Intuitively, λ balances the sparsity of the
 964 solution and prevents overfitting, while higher h offers
 965 a smoother optimization landscape at the expense of
 966 some accuracy. Additionally, all hyperparameter com-
 967 binations have very similar training times. Recall that
 968 all experiments were conducted on a personal laptop,

979 suggesting that training times could be substantially
980 reduced using a compute server.

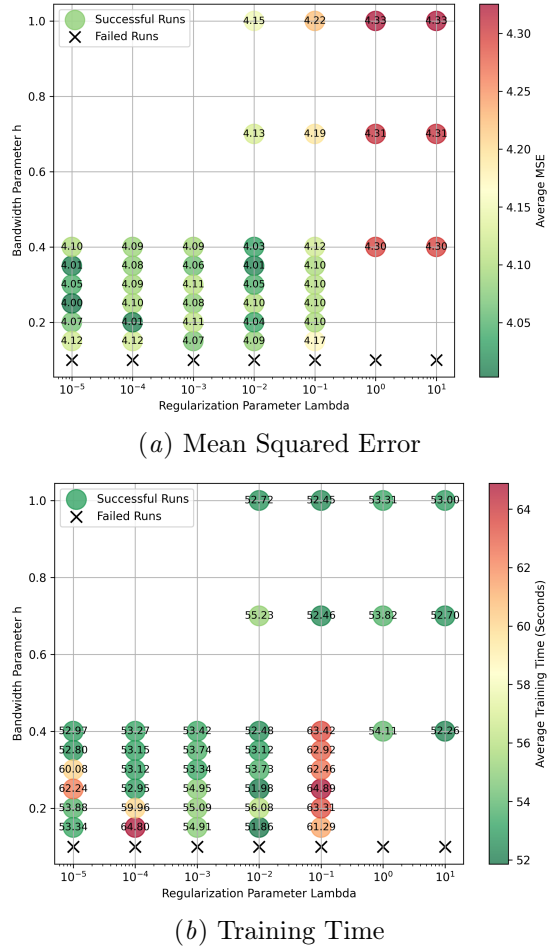


Figure 11: Hyperparameter Sensitivity on IWPC.

981 B.4.2. DIFFERENT OPTIMIZATION ALGORITHMS

982 To assess the sensitivity of our constrained optimization
983 procedure, we perform a comparative analysis
984 of different optimization methods for solving the con-
985 strained problem in our simulation study. For Sce-
986 nario 4, we run experiments using four optimization
987 methods—Tree-based Parzen Estimators (TPE), Dif-
988 fferential Evolution (DE), CMA Evolution Strategy
989 (CMA-ES), and Optuna—across three sample sizes
990 ($n = \{100, 500, 1000\}$), with five repetitions per con-
991 figuration. The performance metrics reported are:
992 total runtime, mean squared error (MSE) of the es-
993 timated heatmap versus ground truth, and the final

994 optimal objective value (as defined in Equation (11)).
995 Our results in Table 3 show that TPE achieves the
996 fastest runtime while yielding comparable MSE error
997 (although not the best) and reasonable objective val-
998 ues at optimality. Notably, DE performs the best in
999 terms of error minimization, but it is also the most
1000 time consuming; therefore, if computational time and
1001 resources are not a limiting factor, DE might be the
1002 preferred option. Conducting the same experiments
1003 in other scenarios yield similar trends.

1004 Appendix C. Comparison with 1005 Existing Methods

1006 To clarify the novelty of our approach and address con-
1007 cerns about its distinction from existing methods, we
1008 provide a comparative analysis of treatment-covariate
1009 interaction learning algorithms. Table 4 summarizes
1010 key attributes, including their ability to handle contin-
1011 uous treatments, classification tasks, interpretability,
1012 and estimation strategies. Unlike prior methods, our
1013 dual-score model offers both optimal treatment rule
1014 estimation and quantitative diagnostic interpretability,
1015 making it particularly suited for clinical applications.

Table 3: Performance Comparison of Optimization Methods for Scenario 4 (Mean \pm Std)

| Method | Runtime (s) | | | Objective Value | | | MSE Heatmap | | |
|--------|-------------------------------------|-------------------------------------|-------------------------------------|-------------------------------------|-------------------------------------|-------------------------------------|-------------------------------------|-------------------------------------|-------------------------------------|
| | n=100 | n=500 | n=1000 | n=100 | n=500 | n=1000 | n=100 | n=500 | n=1000 |
| TPE | 0.353 \pm 0.039 | 1.426 \pm 0.131 | 4.405 \pm 0.169 | 0.075 \pm 0.047 | 0.040 \pm 0.030 | 0.034 \pm 0.024 | 0.149 \pm 0.255 | 0.130 \pm 0.106 | 0.050 \pm 0.030 |
| DE | 0.373 \pm 0.037 | 8.933 \pm 2.226 | 34.930 \pm 9.288 | 0.061 \pm 0.040 | 0.021 \pm 0.018 | 0.021 \pm 0.026 | 0.143 \pm 0.154 | 0.121 \pm 0.215 | 0.032 \pm 0.019 |
| CMA-ES | 0.609 \pm 0.056 | 7.072 \pm 0.383 | 26.004 \pm 2.778 | 0.096 \pm 0.076 | 0.087 \pm 0.094 | 0.063 \pm 0.070 | 0.299 \pm 0.266 | 0.150 \pm 0.112 | 0.134 \pm 0.141 |
| Optuna | 0.911 \pm 0.033 | 2.591 \pm 0.033 | 5.861 \pm 0.501 | 0.063 \pm 0.040 | 0.022 \pm 0.018 | 0.028 \pm 0.026 | 0.145 \pm 0.149 | 0.115 \pm 0.194 | 0.035 \pm 0.022 |

Table 4: Comparison of different algorithms for treatment-covariates interaction learning

| Algorithm | Continuous Treatment | Classification Capability | Optimal Treatment Rule | Quantitative Prognostic Interpretability | Model Estimation | Data Type |
|--|----------------------|---------------------------|------------------------|--|---|-----------------|
| Clause-based Decision List (Zhang et al., 2018) | No | Yes | Yes | No | Kernel Ridge Regression with Q-Learning | Longitudinal |
| AutoGluon (Erickson et al., 2020) | Yes | Yes | No | No | Ensemble Learning | Cross-sectional |
| Decision Trees (Laber and Zhao, 2015) | No | Yes | Yes | No | Tree-based Methods | Cross-sectional |
| SIMSL (Park et al., 2022a) | Yes | No | Yes | No | Spline Regression | Cross-sectional |
| Change-Plane Model (Jin et al., 2023) | No | Yes | No | Yes | Spline Regression | Longitudinal |
| Our Model | Yes | Yes | Yes | Yes | NW Regression | Cross-sectional |